Composite Structures 183 (2018) 550–562

Contents lists available at ScienceDirect

Composite Structures

journal homepage: www.elsevier.com/locate/compstruct

Neural network assisted multiscale analysis for the elastic properties prediction of 3D braided composites under uncertainty

Georgios Balokas [a,*], Steffen Czichon [a], Raimund Rolfes [b]

[a] Structure Development Department, ELAN-AUSY GmbH, Channel 2 Harburger Schloßstr. 24, 21079 Hamburg, Germany
[b] Institute of Structural Analysis, Leibniz Universität Hannover, Appelstraße 9A, 30167 Hannover, Germany

ARTICLE INFO

Article history:
Received 23 January 2017
Revised 1 June 2017
Accepted 13 June 2017
Available online 15 June 2017

Keywords:
Braided composites
Homogenization
Multiscale analysis
Probabilistic analysis
Global sensitivity analysis
Artificial neural networks

ABSTRACT

The stiffness prediction of textile composites has been studied intensively over the last 20 years. It is the complex yarn architecture that adds exceptional properties but also requires computationally expensive methods for the accurate solution of the homogenization problem. Braided composites are of special interest for the aerospace and automotive industry and have thus drawn the attention of many researchers, studying and developing analytical and numerical methods for the extraction of the effective elastic properties. This paper intends to study the effect of uncertainties caused by the automated manufacturing procedure, to the elastic behavior of braided composites. In this direction, a fast FEM-based multiscale algorithm is proposed, allowing for uncertainty introduction and response variability calculation of the macro-scale properties of 3D braided composites, within a Monte Carlo framework. Artificial neural networks are used to reduce the computational effort even more, since they allow for rapid generation of large samples when trained. With this approach it is feasible to apply a variance-based global sensitivity analysis in order to identify the most crucial uncertain parameters through the costly Sobol indices. The proposed method is straightforward, quite accurate and highlights the importance of realistic uncertainty quantification.

1. Introduction

Even though composite materials have been available for several decades already, they are steadily one of the most active engineering research topics. This is justified by their excellent performance in terms of stiffness-to-weight and strength-to-weight ratio, fatigue strength, corrosion resistance, stability and impact properties and numerous other advantages over conventional engineering metals. Composite structures are mainly separated into two categories according to the fiber architecture: laminated composites (a bundle of unidirectional laminas) and 2D or 3D textile composites (where the fibrous reinforcements are interlaced in multi-directions). In textiles, the linear assemblage of the fibers into yarns and the consequent bonding/interlocking of the yarns into specific patterns, add through-the-thickness reinforcement and thus balance between in-plane and out-of-plane properties. A review on textile composites can be found in [1], whereas modeling challenges are investigated and documented in [2]. In [3], a review emphasizing on woven textiles is presented.

Braided composites consist a class of textiles, increasingly used in a wide variety of high-performance industry applications in aerospace, automotive and marine sectors. Braiding can be defined as a composite material preform manufacturing technique where a braiding machine deposits continuous, interwined, fiber tows (yarns) to create desired reinforcing braid architecture before or during the impregnation of the fibers, according to [4]. The combination of an automated and reproducible process together with an excellent rate of material deposition for mass-production of high-level structures, is the main reason for the attention braided composites have received. Nevertheless, analysis of such materials sets challenges and computational obstacles, as it requires very detailed models in order to capture the complexity of braided structures. Review papers on braided describing modeling challenges and trends, can be found in [4,5].

In most problems of engineering and applied mechanics, only the macroscopic mechanical behavior is of interest. However, in composites and generally in heterogeneous materials, the mechanical properties of the individual components along with other lower-scale parameters defining their spatial and size distribution

* Corresponding author.
E-mail address: Georgios.Balokas@elan-ausy.com (G. Balokas).

http://dx.doi.org/10.1016/j.compstruct.2017.06.037
0263-8223/

(e.g. volume fractions etc.), govern in fact the overall mechanical behavior. Hence, attributes of micro and meso scale are extremely important for a better understanding of the elemental properties of those materials. On that account, various modeling approaches for predicting the effective elastic properties of braided composites have been developed, with the intention to describe accurately and efficiently the connection between micromechanical characteristics and macro stiffness properties. A review on the stiffness prediction modeling approaches is offered in [4]. An attractive analytical micromechanics model able to also predict the inelastic and strength behavior (called bridging), is presented in [6], while another analytical model based on numerical simulation and mathematical modeling after analyzing the microstructure of the braided preforms, can be found in [7]. Besides analytical, plenty of numerical multiscale models can be found in the literature, like [8] which is based on the homogenization variational principle and [9] where use of the TexGen mesoscale modeling software is made. In [10], a recent study concerning the friction consideration in a novel interface constitutive model is presented, whereas in [11] a comparison is performed between periodic meshes and a more efficient freely generated mesh of the braided unit-cell. A complete study on elastic prediction of braided composites using both analytical and numerical models is presented in [12]. Recently, an interesting numerical study accounting for the pore defects effect on the elastic properties of braided was offered in [13]. A general information-passing multiscale numerical approach is presented and used in [14,15], enabling material nonlinearity introduction and providing not only stiffness but also strength.

Due to the multiphase and heterogeneous nature of composites, uncertainties are of great substance. Therefore the variability in elastic constants needs to be considered in the mechanical response analysis of composite structures. In principal, uncertainties are classified as either aleatory (inherent randomness in the system) or epistemic (due to partial knowledge of the problem and parameters). A noteworthy attempt to compile and classify the uncertainty modeling approaches for composite structures was made in [16], where it is stated that regarding composite materials, aleatory uncertainty typically refers to fiber and matrix characteristics, manufacturing variations etc., whereas epistemic may be associated with the type of experimental and modeling methods being used. Recent studies [17,18] showed that aleatory uncertainty and specifically fiber waviness, plays an important role in compressive failure of polymer composites by triggering fiber kinking. Significant work regarding the aleatory uncertainty assessment of composite shells and the coupling with current design methods has been performed in [19,20].

Consequently, the scatter in the mechanical properties due to aleatory uncertainty is a dynamic research field, with various approaches considering the probabilistic homogenization problem. Linear perturbation techniques were introduced in [21], while approximate solutions of the elastic response aided by Kriging models were presented in [22]. The influence of random inclusions in the microstructure by applying the extended finite element method (XFEM) was described in [23], whereas the study in [24] established the synergy of Monte Carlo simulation (MCS) and the XFEM for the homogenization problem with random microstructures. A variety of probabilistic approaches in carbon fiber reinforced polymers can be found in [25]. Moreover, the implementation of surrogate (or meta) models becomes a necessity when it comes to the stochastic assessment of such materials. Reviews on neural network (NN) applications in composite materials can be found in [26,27], while a recent review covering a variety of surrogates (polynomial chaos, radial basis functions, Kriging etc.) is presented in [28]. Stochastic optimization is also a field of application for the above models [29,30]. NN have been also used for forming processes simulations [31] while an interesting approach that couples polynomial approximations and NN is offered in [32].

However, the aforementioned work concerns only continuous unidirectional fiber laminate composites. It is only recently that a perturbation technique for the stochastic homogenization of woven composites was proposed in [33], which theoretically could be applied in any textile, though being perturbation-based is limiting information on the shape of the elastic parameters probability density functions (PDFs) and also investigates exclusively uncertainties caused by the material properties of the constituents. A study adding scatter information on braided composites was offered in [34], but it is founded more on model updating based on experimental data, than on probabilistic homogenization modeling for the variability calculation. Also there is not information about the exact source of uncertainty.

In this paper, a probabilistic FEM-based method is proposed for the prediction of the elastic constants of braided composites, under various sources of aleatory uncertainty. The algorithm is based on a Monte Carlo framework so that statistical characteristics of the elastic response can be described in full detail. Uncertainties are covering a wide range of imperfections that can be caused from manufacturing processes, while the numerical tools used in the method allow random properties to be inserted independently. As a result, the effect of every random input can be measured with the aid of a sensitivity analysis technique. With the mesoscale modeler used in the proposed methodology, important geometric properties for a braided material can be taken into account. To further improve the efficiency of the costly Monte Carlo technique and sensitivity analysis, artificial Neural Networks are implemented as surrogate models, decreasing the computational cost by orders of magnitude. The proposed method is applied on a typical triaxial 3D braided model.

2. Homogenization scheme

2.1. Theoretical approach

Consider a macrostructure that is heterogeneous on a lower scale. Let a continuous body of this heterogeneous material denoted M, with multiple phases (Fig. 1). The governing equilibrium and kinematic equations for a solid mechanics problem posed on this structure are:

$$div(\boldsymbol{\sigma}) + \rho\, \boldsymbol{b} = \rho\, \ddot{\boldsymbol{u}} \qquad in\ R \tag{1}$$

$$\boldsymbol{\sigma} = \mathscr{C}\, \boldsymbol{\varepsilon} \tag{2}$$

where $\boldsymbol{\sigma}$ is the stress tensor, $\boldsymbol{\varepsilon}$ is the strain tensor, $\boldsymbol{b}$ are the acting body forces, ρ is the body density and $\mathscr{C}$ is the elasticity tensor of the constitutive equation (Eq. (2)). The essential and natural boundary conditions (BCs) respectively are:

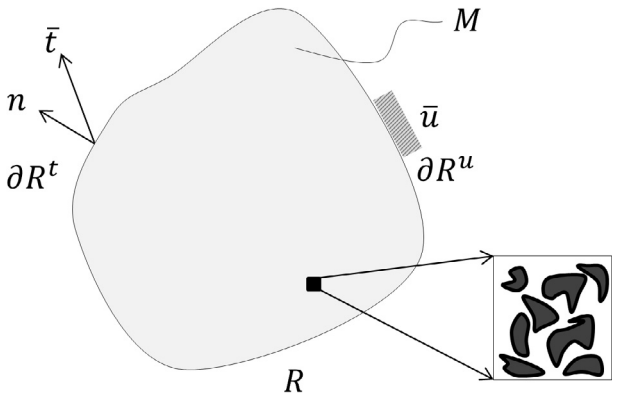

Fig. 1. Heterogeneous material M of the macrostructure in domain R, subjected to essential and natural boundary conditions on surfaces ∂R^u and ∂R^t respectively.

$$\boldsymbol{u} = \bar{\boldsymbol{u}} \qquad on\ \partial R^u \tag{3}$$

$$\boldsymbol{t} = \boldsymbol{\sigma}\,\boldsymbol{n} = \bar{\boldsymbol{t}} \qquad on\ \partial R^t \tag{4}$$

where $\boldsymbol{n}$ is the unit vector normal to the surface ∂R^t where the traction $\bar{\boldsymbol{t}}$ is applied. Due to the presence of heterogeneities, the density and the explicit form of the constitutive equation fluctuate from phase to phase, rendering the solution of the problem very challenging in its original form. The subject of homogenization is the determination of approximate effective quantities ρ^* and $\mathscr{C}^*$, so that the problem of the homogeneous effective material M^* with the same BCs would be solvable.

In essence, the homogenization process is performed on a representative volume element (RVE) of the heterogeneous material which is defined by Hill [35] as the smallest sample entirely typical of the whole mixture on average. So after several averaging procedures, the homogenization problem degenerates to the following RVE problem under quasistatic conditions:

Determine $\boldsymbol{u}$ so that:

$$div(\boldsymbol{\sigma}) = 0 \quad in\ volume\ V\ of\ RVE \tag{5}$$

subject to BCs such that:

$$\boldsymbol{\sigma}^* \cdot \boldsymbol{\varepsilon}^* = \frac{1}{|V|}\int_V \boldsymbol{\sigma}\cdot\boldsymbol{\varepsilon}\, dV \tag{6}$$

Eq. (6) is known as the Hill's energy averaging theorem and states that the strain energy of the homogenized macrocontinuum, with macroscopic stress and strain tensors $\boldsymbol{\sigma}^*$ and $\boldsymbol{\varepsilon}^*$ respectively, has to be equal to that of the microstructured RVE, with $\boldsymbol{\sigma}$ and $\boldsymbol{\varepsilon}$ being the corresponding microscopic quantities.

When the solution of the previous problem is obtained, the effective constitutive formulation is determined by relating $\boldsymbol{\sigma}^*$ to $\boldsymbol{\varepsilon}^*$. For an elastic orthotropic material, the generalized stress–strain constitutive law of Eq. (2) is given via:

$$\begin{Bmatrix}\sigma_1\\ \sigma_2\\ \sigma_3\\ \tau_{23}\\ \tau_{31}\\ \tau_{12}\end{Bmatrix} = \begin{bmatrix}\mathscr{C}_{11} & \mathscr{C}_{12} & \mathscr{C}_{13} & 0 & 0 & 0\\ \mathscr{C}_{21} & \mathscr{C}_{22} & \mathscr{C}_{23} & 0 & 0 & 0\\ \mathscr{C}_{31} & \mathscr{C}_{32} & \mathscr{C}_{33} & 0 & 0 & 0\\ 0 & 0 & 0 & \mathscr{C}_{44} & 0 & 0\\ 0 & 0 & 0 & 0 & \mathscr{C}_{55} & 0\\ 0 & 0 & 0 & 0 & 0 & \mathscr{C}_{66}\end{bmatrix}\begin{Bmatrix}\varepsilon_1\\ \varepsilon_2\\ \varepsilon_3\\ \gamma_{23}\\ \gamma_{31}\\ \gamma_{12}\end{Bmatrix} \tag{7}$$

The inverse of the macroscopic stiffness matrix $\boldsymbol{S} = \mathscr{C}^{-1}$ is the compliance (or flexibility) matrix. The elastic properties can be determined from compliance constants by applying separately uniaxial normal/shear stresses in each direction/plane and restricting the remaining degrees of freedom. The compliance matrix as a function of the engineering constants has the following form:

$$\begin{Bmatrix}\varepsilon_1\\ \varepsilon_2\\ \varepsilon_3\\ \gamma_{23}\\ \gamma_{31}\\ \gamma_{12}\end{Bmatrix} = \begin{bmatrix}\frac{1}{E_1} & -\frac{\nu_{21}}{E_2} & -\frac{\nu_{31}}{E_3} & 0 & 0 & 0\\ -\frac{\nu_{12}}{E_1} & \frac{1}{E_2} & -\frac{\nu_{32}}{E_3} & 0 & 0 & 0\\ -\frac{\nu_{13}}{E_1} & -\frac{\nu_{23}}{E_3} & \frac{1}{E_3} & 0 & 0 & 0\\ 0 & 0 & 0 & \frac{1}{G_{23}} & 0 & 0\\ 0 & 0 & 0 & 0 & \frac{1}{G_{31}} & 0\\ 0 & 0 & 0 & 0 & 0 & \frac{1}{G_{12}}\end{bmatrix}\begin{Bmatrix}\sigma_1\\ \sigma_2\\ \sigma_3\\ \tau_{23}\\ \tau_{31}\\ \tau_{12}\end{Bmatrix} \tag{8}$$

The compliance matrix is naturally symmetric due to Maxwell's reciprocal theorem:

$$\frac{\nu_{ij}}{E_i} = \frac{\nu_{ji}}{E_j} \tag{9}$$

2.2. Numerical implementation

This study employs the open-source software TexGen [36] for the treatment of the homogenization problem. TexGen is a 3D solid modeler of textile structures at unit-cell level, developed at the University of Nottingham. It allows user-friendly modeling of the complex yarn architecture through either graphical user interface or Python scripting. The fact that yarns are simulated as solid volumes representing the approximate bounds of the fibers contained within them, makes the modeling feasible through simply defining the path nodes and the cross-section of the yarns.

TexGen approaches the unit-cell according to the principles documented in [37], where only translational symmetry transformations are employed (reflectional or rotational symmetries are excluded). This results in major advantages, as the unit-cell can be subjected to arbitrary combinations of macroscopic stresses and strains with a single set of BCs, but also can be applicable to nonlinear problems of any nature. Periodic BCs are applied on the unit-cell in order to satisfy Eq. (6), based on the following relations between the macroscopic strains and the relative displacements at a point P in the unit-cell to those at P' as the image of P in another cell:

$$\begin{aligned} u' - u &= (x'-x)\varepsilon_x^0 + (y'-y)\gamma_{xy}^0 + (z'-z)\gamma_{xz}^0\\ v' - v &= (y'-y)\varepsilon_y^0 + (z'-z)\gamma_{yz}^0\\ w' - w &= (z'-z)\varepsilon_z^0 \end{aligned} \tag{10}$$

where x, y and z are the coordinates of point P, u, v and w are the displacements at the same point, the respective symbols with an apostrophe are associated with the point P' (an image of P) and $\varepsilon_x^0, \varepsilon_y^0, \varepsilon_z^0, \gamma_{yz}^0, \gamma_{xz}^0, \gamma_{xy}^0$ are the macroscopic strains. In obtaining the displacement field of Eq. (10), the following kinematic constraints are applied:

$$\begin{aligned} &u = v = w = 0\\ &\frac{\partial w}{\partial x} = \frac{\partial v}{\partial x} = \frac{\partial w}{\partial y} \qquad at\ \ x = y = z = 0 \end{aligned} \tag{11}$$

The exact procedure on how to derive the periodic BCs from this formulation, is referred to [37].

TexGen has the ability to automatically produce an input file for the ABAQUS commercial FE package [38], including all necessary data about geometry, materials and support of the unit-cell. The ABAQUS implementation of the periodic BCs involves the use of an equation for the representation of the relative displacement of two node sets at opposite boundaries (faces, edges etc.), equal to the displacement of a dummy node. In this manner the unit-cell deformation is controlled by applying BCs to the dummy node.

Regarding the elastic properties extraction, concentrated loads are applied on those dummy nodes separately in every necessary direction, which are related to the macroscopic stresses through virtual work equilibrium [37]. For example, if a force F_x is applied to the degree of freedom ε_x^0 of a unit-cell while all the other extra degrees of freedom are free from constraints, the work done by the force is:

$$W = \frac{1}{2}F_x\varepsilon_x^0 \tag{12}$$

The strain energy stored in the unit-cell can be expressed in terms of the macroscopic stresses and strains as:

$$E = \frac{1}{2}\int_V \sigma_x^0\varepsilon_x^0\, dV = \frac{1}{2}V\sigma_x^0\varepsilon_x^0 \tag{13}$$

where σ_x^0 is the macroscopic normal X stress and V is the unit-cell volume. Equating W to E results in the following relationship for the X-direction:

$$\sigma_x^0 = \frac{F_x}{V} \tag{14}$$

The effective longitudinal modulus of the material would then be obtained as:

$$E_x^0 = \frac{\sigma_x^0}{\varepsilon_x^0} = \frac{F_x}{V\varepsilon_x^0} \quad \text{when} \quad F_y = F_z = F_{yz} = F_{zx} = F_{xy} = 0 \tag{15}$$

The forces are applied volumetrically so that all stresses similar to Eq. (14) would be unitary. As a result, the displacement output from the FE analysis at the dummy nodes will represent the strain and according to Eq. (15), the moduli would simply be the inverse of calculated strains. The remaining effective properties for an orthotropic material are obtained accordingly (six load cases in total).

3. Global sensitivity analysis for Monte Carlo simulation

The inherent probabilistic nature of most design parameters hampers the deterministic treatment of engineering problems and leads to analysis under uncertainty. In a probabilistic model with multiple discrete sources of uncertainty, sensitivity analysis offers the impact of each random input to the total output variability of the model. Hence, the system complexity can be reduced and the cause-and-effect relationship can be explained.

This paper applies a variance-based global sensitivity analysis (GSA) that is able to describe the sensitivity pattern of a model, through a full decomposition of the output variance into terms corresponding to the input parameters and their interactions. The principal advantages of such techniques over local sensitivity analyses are the consideration of the whole input space, the applicability in nonlinear responses and the ability to measure effects of interaction in non-additive systems [39].

3.1. Formulation

Consider a model $y = f(x_1, x_2, \dots\ x_k)$ with y a scalar. Given that f is a square integrable function over the k-dimensional unit hypercube Ω^k, the model may be decomposed in the following way [40]:

$$f = f_0 + \sum_i f_i + \sum_{j>i} f_{ij} + \ldots + f_{12\ldots k} \tag{16}$$

where $f_i = f_i(x_i), f_{ij} = f_{ij}(x_i, x_j)$ etc. All the terms in the functional decomposition are orthogonal. Consequently, they can be calculated using the conditional expectations of the model output y as:

$$\begin{aligned} f_0 &= E(y) \\ f_i &= E(y|x_i) - E(y) \\ f_{ij} &= E(y|x_i, x_j) - f_i - f_j - E(y) \end{aligned} \tag{17}$$

If Eq. (16) is squared and integrated, appears the expression:

$$\int f^2 d\boldsymbol{x} - f_0^2 = \sum_i \int f_i^2 dx_i + \sum_{j>i} \int f_{ij}^2 dx_i dx_j + \ldots + \int f_{12\ldots k}^2 dx_1 dx_2 \ldots dx_k \tag{18}$$

The left part of Eq. (18) is the total variance of output y and the terms of the right part are decomposed variance terms with respect to the sets of the input x_i. With the aid of Eq. (17) the final expression for the variance decomposition is reached:

$$\begin{aligned} Var(y) &= \sum_{i=1}^{k} V_i + \sum_{j>i}^{k} V_{ij} + \cdots + V_{12\ldots k} \\ \text{where} \quad V_i &= Var_{x_i}(E_{x_{\sim i}}(y|x_i)) \\ V_{ij} &= Var_{x_{ij}}(E_{x_{\sim ij}}(y|x_i, x_j)) - V_i - V_j \quad etc. \end{aligned} \tag{19}$$

The $x_{\sim i}$ notation indicates the set of all variables except x_i. A direct variance-based measure of sensitivity called first-order sensitivity index or first order Sobol index, can be obtained by dividing the term of interest from the decomposed variance by the unconditional variance $Var(y)$:

$$S_i = \frac{V_i}{Var(y)} \tag{20}$$

This is the contribution to the output variance of the main effect of x_i, therefore it measures the effect of varying x_i alone, but averaged over variations in other input parameters. It is normalized by the total variance to provide a fractional contribution.

3.2. Monte Carlo implementation

In the majority of cases, the model does not allow for an analytical evaluation of the integrals in the variance decomposition. Thus, GSA is performed through estimators for the Sobol indices, emerging from a sampling technique within a Monte Carlo framework. A summary of the estimators described so far in the literature is documented in [41]. In this paper we use the following estimator for the first order index:

$$V_i = Var_{x_i}(E_{x_{\sim i}}(y|x_i)) \approx \frac{1}{N}\sum_{j=1}^{N} f(B)_j (f(A_B^i)_j - f(A)_j) \tag{21}$$

In the above equation, N is the problem-dependent base sample (large enough sample size for the Monte Carlo procedure to converge) and $f(A), f(B), f(A_B^i)$ are the model outputs of the input matrices A, B and A_B^i respectively. The sample matrices are generated as follows [39]: A and B are two (N, k) matrices with random sample points of the input space, where k is the number of random inputs. Matrix A_B^i is identical with A, except that its ith column is substituted with the ith column of B $(i = 1, \ldots, k)$. As a result, k matrices similar to A_B^i are required, which leads to a total computational cost of $N(k+2)$ simulations.

The accuracy of the estimators is highly dependent on N. So computational expense is a problem when the model needs considerable time for a single simulation (e.g. FE model). In addition, the convergence of the Sobol index (Eq. (20)) might require a large sample N when approximated with an estimator (Eq. (21)), regardless if the crude Monte Carlo problem has already converged for a smaller size. The potential excessive cost of the Sobol indices has guided researchers to alternative techniques, like polynomial chaos expansions [42,43].

4. Artificial neural networks

Artificial neural networks, or simply neural networks (NN), are mathematical models based on biological nervous systems, with the ability to learn their environment by example through training via samples. In principal, they are used as a Machine Learning method for a variety of applications, such as prediction, pattern recognition, decision making etc. For engineering mechanics, they are mostly considered as surrogate (or meta) models for the rapid mapping between given input and output quantities. Their massively parallel structure composes a very fast information-processing mechanism, which can enhance the efficiency of numerical simulations by producing extreme amount of results with trivial computational effort. As a result, the use of NN can practically eliminate any limitation on the scale of the problem and the sample size used for MCS.

4.1. Basic neural network structure

A neural network consists of at least three layers: the input, the output and one hidden layer. In general there might be several hidden layers. Terminology is borrowed from neuroscience, as the units (nodes) inside every layer are called neurons, while the links between them are called synapses. Although there are numerous

different NN architectures (e.g. radial basis function networks, Kohonen self-organizing networks, recurrent networks among others [44]), the most commonly used for surrogate modeling in engineering are the multilayer feed-forward NN.

A typical configuration of a single layer feed-forward network is demonstrated in Fig. 2. The input neurons (squares) do not process information and only connect the network to the external environment, as terminal points. The neurons of the hidden layer (circles) process information coming from a previous layer and feed their output to the next layer. The hidden denotation originates from the lack of directly observable data. Thus, information is propagated in a single direction, from the input data towards the output (feed-forward). It is noted that there is no connection among neurons of the same layer.

Regarding the processing neurons, their interior structure is summarized in the lower part of Fig. 2. For every connection between neurons there is a weight parameter w_{ij}, which corresponds to the influence of each of the preceding neurons. Every input x_i received by the neuron is multiplied with the corresponding weight and then the sum of those products is calculated by the following formula:

$$z_j = \sum_{i=1}^{n} x_i w_{ij} + b \tag{22}$$

where b is a bias term allowing the neuron to cover a wider range. The result is sent through a nonlinear transfer function called activation function, where the nonlinearity of the decision boundary is introduced. Common activation functions are the sign function and sigmoid functions like the logistic or the hyperbolic tangent function etc.

4.2. Training process

Training a NN is a challenging task, as the problem of overfitting is lurking. The learning procedure is based on a general function optimization problem, where the weights are adjusted in order for the mapping to approximate closely the training set. The objective function is the sum squared error between the predicted output $t(\boldsymbol{w})$ and the target output y_0:

$$E(w_{ij}) = \frac{1}{2}\sum [t(w_{ij}) - y_0]^2 \tag{23}$$

In the minimization process, the weights of all the synapses are modified until the desired error level is achieved or the maximum number of cycles is reached. The weights are updated through an iterative procedure:

$$w_{ij}^{(t+1)} = w_{ij}^{(t)} + \Delta w_{ij} \tag{24}$$

where Δw_{ij} is the correction of the weight at the tth learning step, which is calculated by the following formula:

$$\Delta w_{ij} = -n\frac{\partial E}{\partial w_{ij}} \tag{25}$$

where n is a small parameter adjusting the correction each time, called learning rate. The algorithm described above is called backpropagation algorithm [44].

The definition of overfitting is the poor generalization ability of a NN despite the very small error prediction over the training data. The learning process is so powerful that guides the NN to learn the train data "too well". However, due to the large amount of neurons involved, the error for new predictions (outside the training data) is large. An illustrative example is given in Fig. 3 for the 2D space (scalar input and output), where an overfitting of the training sample (Fig. 3a) is contradicted with a good fit for the exact same data (Fig. 3b).

There are several methods able to rectify the overfitting problem, with the most popular among others being the early stopping of the training and the regularization of the error function [45]. The first one involves a fraction of the sample data being used as a validation dataset, whose error is monitored over the iterations and stops training if its value increases rapidly. Regularization is the intention to smoothen the network's response by modifying the objective function. The idea emerged because of the excessive output variability observed by large weights.

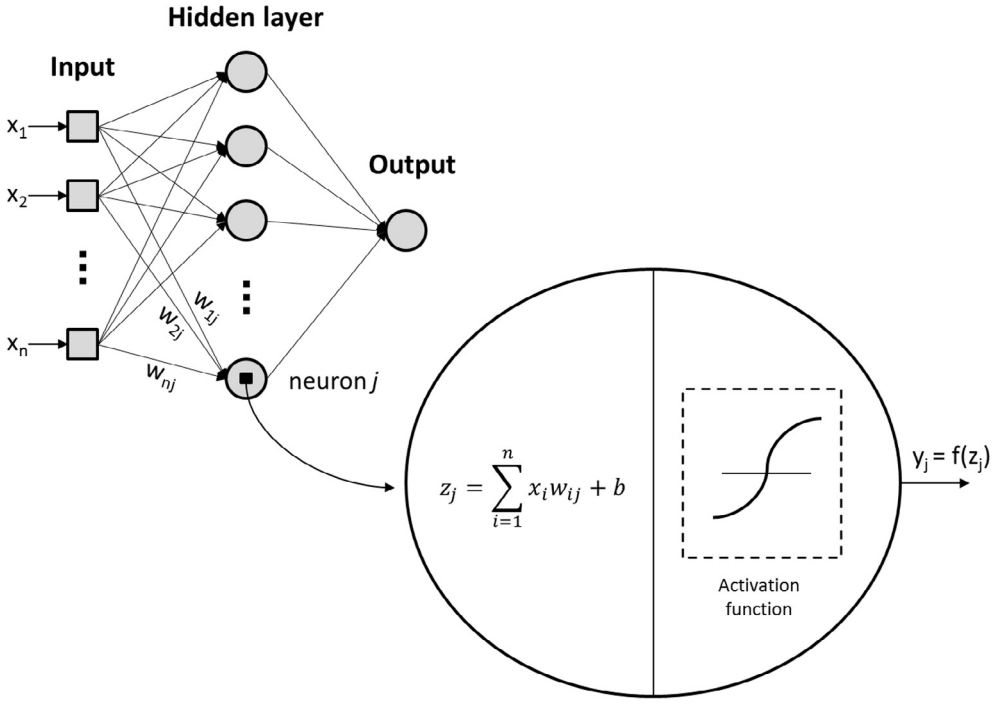

Fig. 2. Architecture of a single layer feed-forward network and neuron structure.

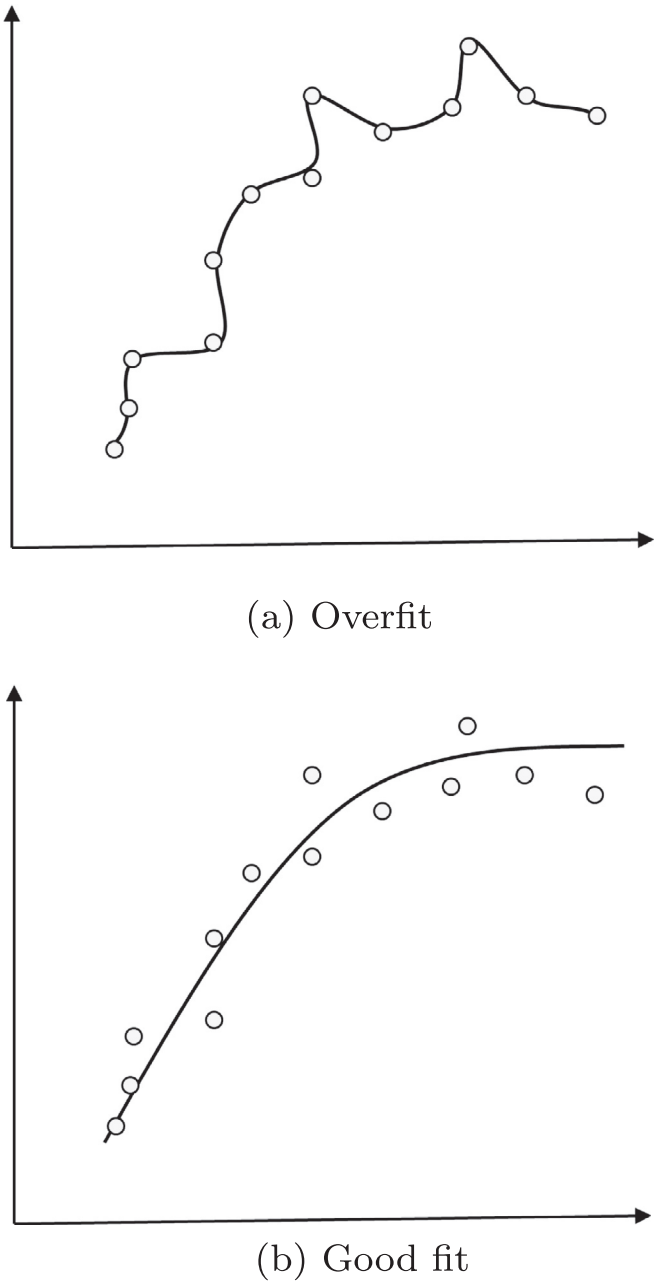

Fig. 3. Overfitting example.

5. Proposed methodology

As mentioned in the introduction, the proposed method is used for the probabilistic analysis of 3D braided composite structures in a Monte Carlo framework. However, it is not limited on braided because the use of TexGen as a modeler allows for any kind of textile composite. Even though the problem is linear, the method is based on the versatile tool of MCS and is, therefore, able to calculate the complete PDF of the response (not just low order moments or probabilities of exceedance of a prescribed value etc.).

Moreover, the method not only allows for material property related uncertainties, but also for geometric uncertainties at the unit-cell level, such as braid and undulation angles. Uncertainties are distinct and due to the clear boundaries between the scales, the variability propagation towards higher levels can be predicted. The division of the uncertainties enables sensitivity analysis and subsequently offers the identification of the parameter with the most crucial effect. The algorithm is quite efficient but the performance is further accelerated by using NN for the repetitive procedure of MCS.

5.1. Multiscale algorithm

Python scripting provides great synergy between the preprocessing in TexGen and the post-processing in ABAQUS. Hence, the algorithm can be implemented in Python in a straightforward manner. The parametric geometrical model of the unit-cell at the mesoscale is scripted with the functions provided by TexGen, with respect to geometric variable of interest, which will be potentially used as an uncertainty. Building a unit-cell textile model requires definition of the yarn paths, the yarn cross-sections and the yarn repeats within a domain. Since the model simulates the yarns as solids, homogenization of their material properties needs to be performed.

The algorithm is much faster if analytical expressions for the microscale material behavior are used and since the Chamis model [46] has been found quite accurate for laminate composites, it is applied for the micro-to-meso scale transition. The yarns in a textile-based composite are essentially unidirectional continuous fiber composites, so the applicability of the model is valid. The transversely isotropic properties of the yarn according to the Chamis model are governed by the following expressions:

$$\begin{aligned} E_{11} &= V_f E_{f,11} + (1 - V_f) E_m \\ E_{22} = E_{33} &= \frac{E_m}{1 - \sqrt{V_f}\left(1 - \frac{E_m}{E_{f,22}}\right)} \\ G_{13} = G_{12} &= \frac{G_m}{1 - \sqrt{V_f}\left(1 - \frac{G_m}{G_{f,12}}\right)} \\ G_{23} &= \frac{G_m}{1 - V_f\left(1 - \frac{G_m}{G_{f,23}}\right)} \\ \nu_{12} = \nu_{13} &= \nu_m + V_f(\nu_{f,12} - \nu_m) \\ \nu_{23} &= V_f \nu_{f,23} + V_m\left(2\nu_m - \frac{\nu_{12}}{E_{11}} E_{22}\right) \end{aligned} \tag{26}$$

where $E_{f,11}, E_{f,22}, G_{f,12}, G_{f,23}, \nu_{f,12}$ and $\nu_{f,23}$ are the transversely isotropic material properties of the fibers, E_m, G_m and ν_m are the isotropic material properties of the polymer matrix and V_f is the yarn volume fraction (percentage of the volume of fibers inside the volume of the yarn).

The next step is to call ABAQUS via Python, for the FE solution of the input file generated by TexGen. It is noted that a mesh convergence study is necessary for the trade-off between accuracy and efficiency in order to adjust the voxel mesh parameters of the unit-cell. Once the model is solved, the effective elastic properties of the macroscale (assumed orthotropic) are extracted with a script implementing the process described in Section 2.2. The procedure described so far needs to be automated in order to generate a sample through Monte Carlo analysis.

The generated sample is used as a training dataset for a NN in MATLAB [47]. An early stopping method is used in order to further improve generalization. In this technique, which is enclosed in MATLAB NN tool, the available data are divided into three subsets: the training, validation and testing set. The training set is used for the procedure described in Section 4.2 (gradient computation and weights updating). The validation set is used as a separate dataset whose error is monitored during the training, so that the generalization performance is evaluated. During the initial phase of training the validation error normally decreases, along with the training error. When the network begins to overfit the data, the validation

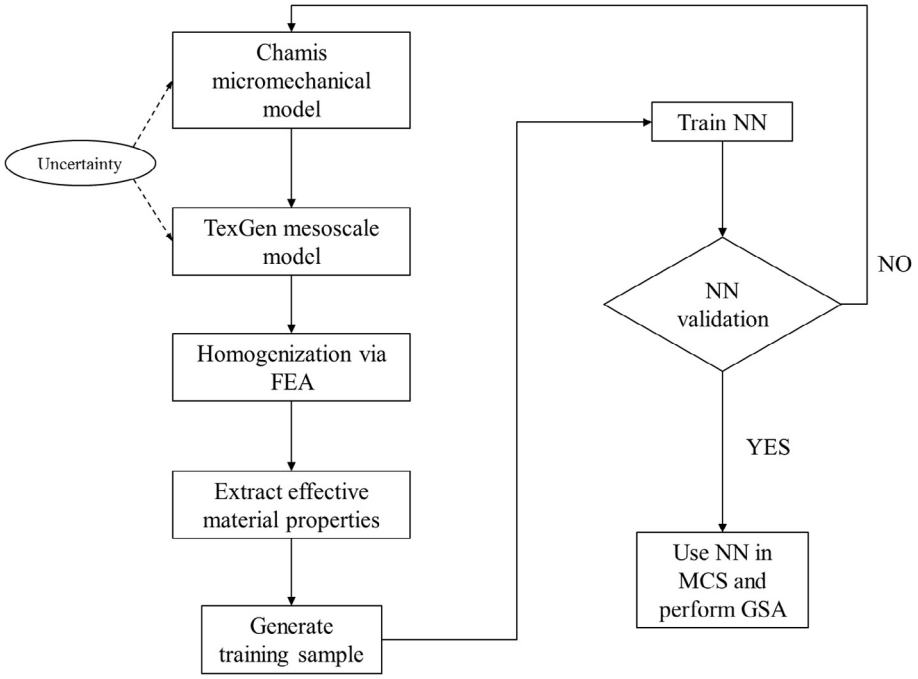

Fig. 4. A flow chart of the proposed methodology.

error begins to rise and the training process is stopped. The weights and biases at the minimum error are adopted. Finally, the testing dataset is used strictly after the training process has finished and offers a representative error which can be expected from absolutely new data. In our study, the input data are randomly divided so that 70% of the samples are assigned to the training set, 15% to the validation set and 15% to the testing set.

Afterwards, the NN is evaluated through a target value for the mean squared error of the prediction. If the criterion is met, the NN is used for the MCS, enabling the fast extraction of excessive response samples for the effective material properties. Furthermore, a GSA framework for the calculation of the Sobol indices can be scripted, for the case of a vector input of uncertainties, according to the formulation of Section 3. If the error is larger than the threshold, the NN needs to be redesigned, either in terms of a new dataset or number of layers and neurons.

A schematic description of the aforementioned methodology is presented in Fig. 4. Uncertainties can be introduced either in the microscale (Chamis micromechanical model), or in the mesoscale through parametric scripting for the unit-cell geometry. As mentioned previously, at least the left part of the chart is required to be automated, as the training of the NN could be performed manually. Nevertheless, it is considered much more efficient to automate the entire algorithm by coupling Python with the MATLAB NN tool. The post-processing for the calculation of the Sobol sensitivity indices is also scripted in Python.

5.2. Experimental validation

The combination of Chamis model, TexGen and ABAQUS for the numerical extraction of the elastic properties, is validated through selected experimental results studied in [48]. This study obtained, among others, the mechanical properties of a triaxial braided carbon/epoxy composite and investigated the effect of the braid angle. Three different braid architectures with a braid angle of $30^{\circ}, 45^{\circ}$ and 60° are each tested in their longitudinal and transverse direction. The values for these cases are presented in Fig. 5 in comparison with the numerical prediction of the multiscale modeling, represented by the solid lines, for the cases of E_1 and E_2. The accuracy is satisfactory, even though there are some approximation errors introduced by the scaling of the results due to volume fraction discrepancies.

6. Numerical examples

6.1. Model description

The model examined herein, can be specified as a typical 3D triaxial braided composite. Triaxial means that the yarns run in three directions. The axial (or warp) yarns lay straight and equally spaced, while the weft yarns interlace the axial yarns at an angle, according to the pattern shown in Fig. 6a. The layer architecture is based on a CT scan conducted on a braided tubular structure.

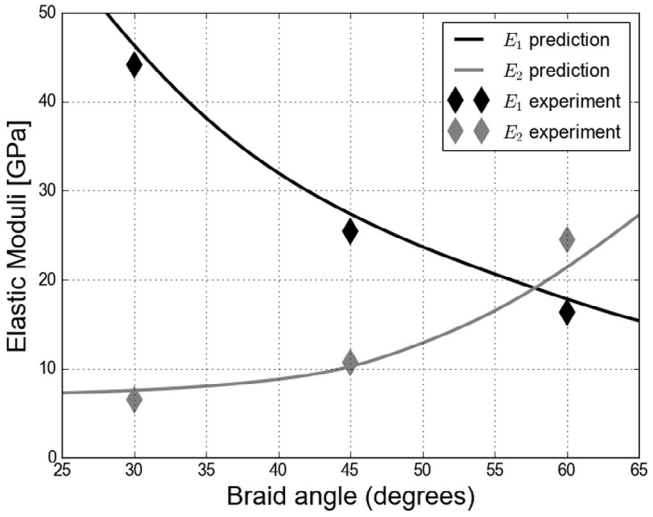

Fig. 5. Comparison of the proposed multiscale methodology (solid lines) with experimental values.

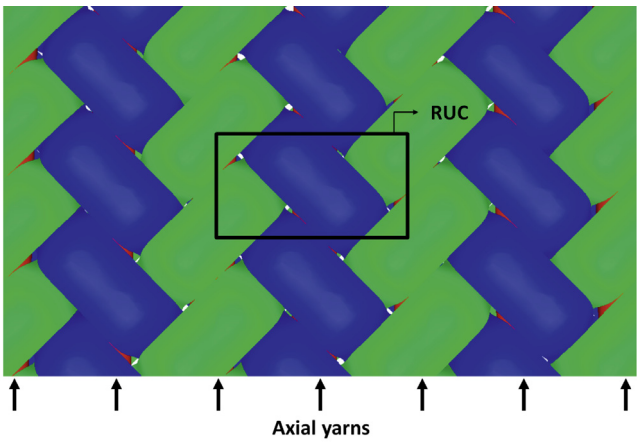

(a) Braiding pattern and RUC

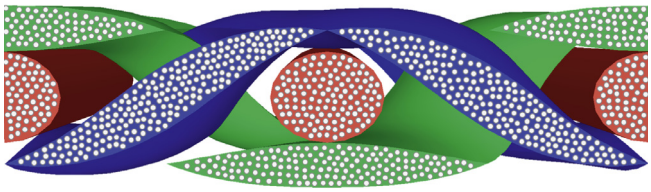

(b) Cross-section

Fig. 6. Triaxial braiding pattern: (a) Top view, (b) Side view (cross-section)

A cross-section of the braiding pattern is presented in Fig. 6b, where the heterogeneity of the yarns is emphasized by illustrating the embedded fibers. The section area of the weft yarns (green and blue) is lenticular (intersection of two circles), while the axial yarns (red) are of elliptical shape.

The representative unit-cell (RUC) extracted from the braiding pattern for the TexGen modeling (Fig. 6a) is presented in Fig. 7a in an isometric projection. The in-plane angle between the weft yarn and the axial yarn is the braid angle (BA) and the out-of-plane angle that the weft yarns are forming within the cell thickness, is the undulation angle (UA). These two geometric variables consist the most significant structural parameters of the mesoscale for a braided composite, considering that they are fully correlated with the unit-cell volume fraction (percentage of the volume of yarns inside the volume of the unit-cell). Fig. 7b presents the meshed unit-cell model in ABAQUS (matrix is excluded for visibility reasons). Characteristics from AS4 Carbon Fibers and EPON 9504 resin for the polymer matrix are used. Material properties selected from [49], are summarized together with the mesoscale geometric properties in Table 1.

Table 1
Material and geometric parameters of braided model.

Parameter	Mean value
Longitudinal fiber modulus E_{f1}	227.53 GPa
Transverse fiber modulus E_{f2}	16.55 GPa
Shear fiber modulus G_{f12}	24.82 GPa
Shear fiber modulus G_{f23}	6.89 GPa
Fiber Poisson's ratio ν_{12}	0.2
Fiber Poisson's ratio ν_{23}	0.25
Matrix Young's modulus E_m	3.5 GPa
Matrix Poisson's ratio ν_m	0.38
Yarn volume fraction (YVF)	70%
Braid angle (BA)	45°
Undulation angle (UA)	57°

6.2. Microscale uncertainty – A single case

As mentioned in Section 5.1, uncertainties could be introduced either in the microscale through the Chamis model (fiber/matrix properties, volume fraction etc.), or in the mesoscale through parametric scripting for the geometric parameters of interest (braid and undulation angles, yarn section shapes etc.), which have a direct impact on the unit-cell volume fraction and consequently the effective macro properties. In this section, the yarn volume fraction (V_f in Eq. (26)) is considered as an uncertainty and we present its effect to the output macro-properties, from a statistical point of view.

Despite the fact that most of the uncertain quantities appearing in practical engineering problems are non-Gaussian in nature, the Gaussian assumption is often used due to its simplicity and the lack of relevant experimental data. To that end, the yarn volume fraction is modeled as a Gaussian random variable, with mean value according to Table 1 and coefficient of variation (COV) equal to 10%. COV is defined as the ratio of the standard deviation over the mean value and is used in this study as a unitless measure for both input and output variability, representing the second statistical moment.

Fig. 8 presents the required simulations for a sufficient representation of the COV of the effective macroscopic properties. As shown, statistical convergence is practically achieved after 400 simulations, which means that for the PDF roughly 1000 simulations would surely be an adequate estimation. The evolution of the mean value is not presented since the convergence is almost instant.

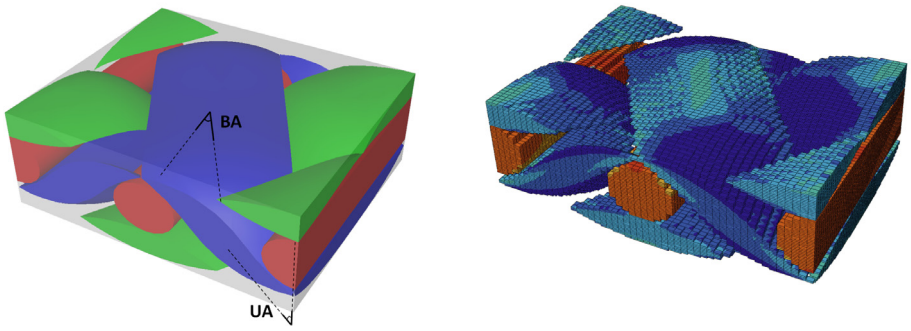

(a) TexGen model (b) FE model

Fig. 7. Representative unit-cell mesoscale model.

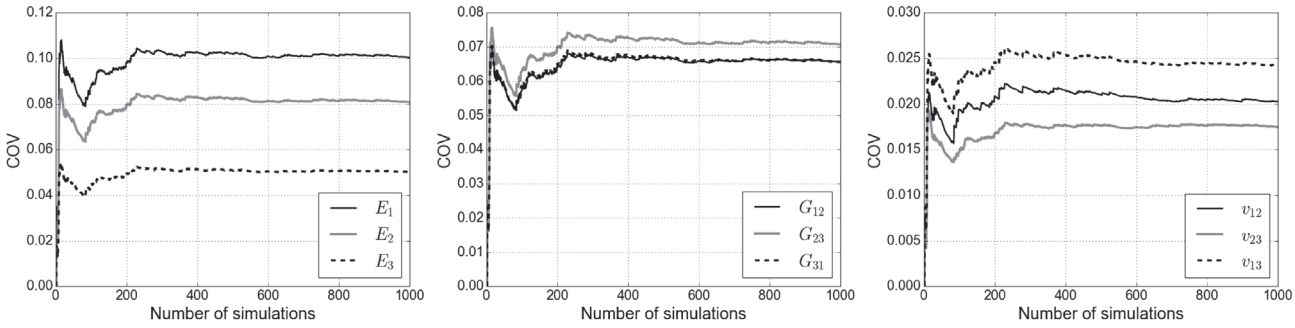

Fig. 8. Statistical convergence of COV for the effective properties.

The response PDFs are calculated with the aid of the kernel density estimation method (KDE), which is a fundamental data smoothing technique, where inferences about the population are made based on a finite data sample [50]. In Fig. 9, we compare the response after 1000 crude MCS (which is considered as a reference solution) and after 1000 simulations with a trained NN, according to the methodology described in Section 5.1, for E_1, E_2 and E_3. It is observed that the accuracy of the NN-assisted algorithm is very good, providing that the NN is well trained. In general, the problem described in this paper does not need more than one hidden layer for good NN performance. On average, a training sample of 40–60 input/output sets is sufficient and the neurons should not be more than 10. The exact number of neurons is always dependent on the size of the training sample. In Fig. 10a, an illustrative error plot of the data sets against the internal iterations of a well trained NN is presented, while the convergence of the response with respect to the size of the sample used for training is presented in Fig. 10b in terms of cumulative distribution functions (CDFs) and in Fig. 10c in terms of PDFs. All three plots correspond to the response of the longitudinal modulus E_1, while

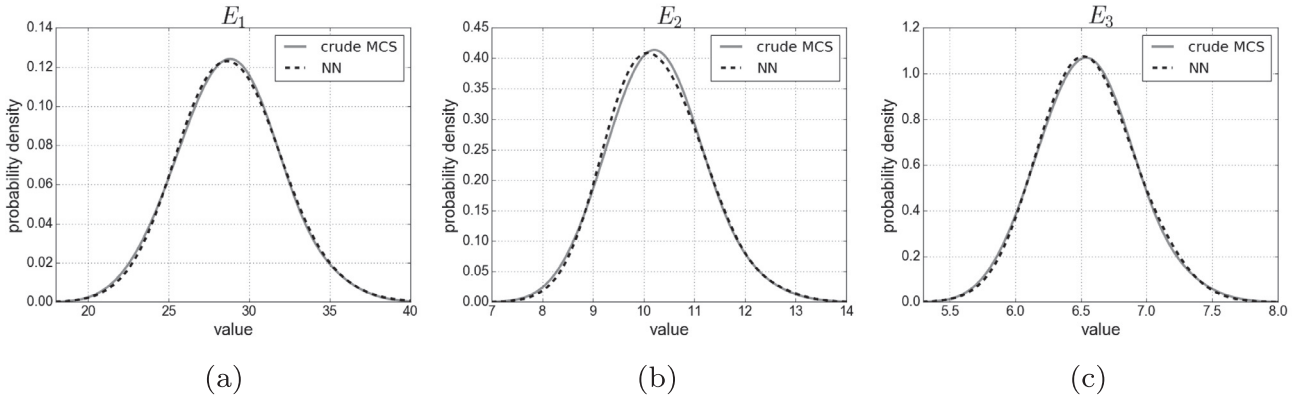

Fig. 9. Accuracy of the proposed NN-aided method (values in GPa).

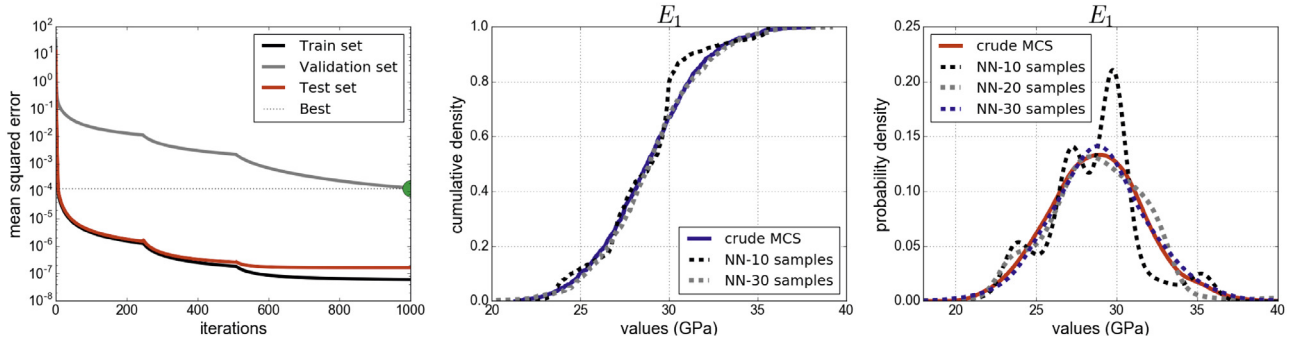

Fig. 10. Training information.

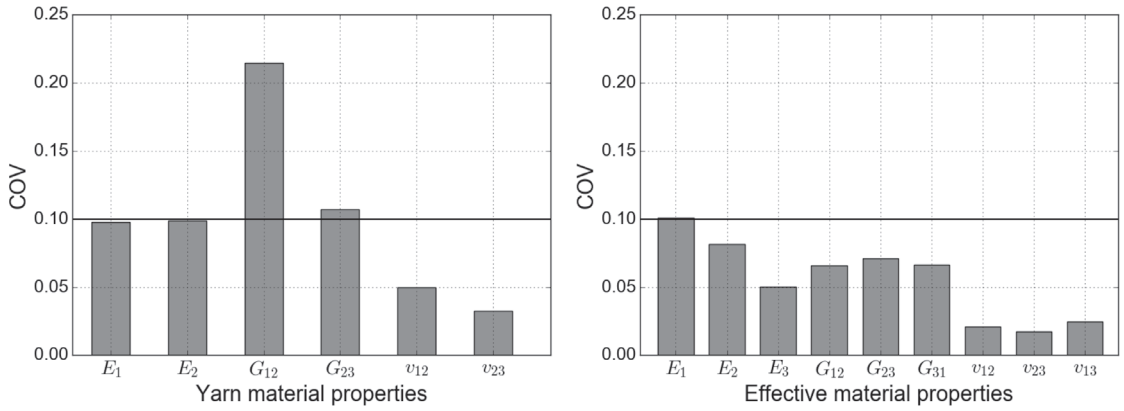

(a) Mesoscale variability (b) Macroscale variability

Fig. 11. Variability propagation through the scales.

the hidden layer holds 5 neurons for this case. Naturally, convergence can be achieved more easily for the CDF case, since the data are going through an additional integration procedure.

To further boost the training procedure, a Latin Hypercube Sampling (LHS) technique could be used for a more efficient choice of the input sample, as the random variables are sampled from the complete range of their possible values, ensuring a smaller sample size is required [51]. Since the relation between the elastic properties and the V_f is almost linear [52], the PDF shape in Fig. 9 is Gaussian. Skewness is expected to be introduced by other uncertain parameters, like the braid and undulation angles, where the relation is nonlinear as in Fig. 5 (see also [12,48,53]), in case they dominate the response. In terms of efficiency, an Intel Core i7-3770 processor required 195600 s (3260 min) for 1000 crude MCS realizations, while 1000 realizations with a trained NN were performed in 10.53 s (0.1755 min).

Regarding the uncertainty propagation, the response variability is calculated in both the mesoscale and the macroscale phase. Results are illustrated in bar charts for all material properties involved, in Fig. 11. An horizontal solid line is drawn at the COV level of 10% as a reference to the input variation. It is worth noting the slight reduction of the variability through the scales, especially the high G_{12} variability of the yarns in the mesoscale, which however does not increase the output samples of the macroscale.

6.3. Sensitivity analysis – General case

The efficiency provided by the NN, enables the application of the variance-based GSA described in Section 3, since it is costless to perform the large number of simulations required for the convergence of the Sobol index estimation. Several uncertain parameters are considered herein and through the total output variance decomposition, it is straightforward to draw conclusions about the statistical importance and impact of each input.

The selected random input parameters are inspired from possible uncertainties caused by manufacturing procedures. We choose the following 6 random properties from Table 1: E_{f1}, E_{f2}, G_{f12}, YVF, BA and UA. The first four parameters are introduced in the microscale, while the last two in the mesoscale and they are all considered as the most influential according to some preliminary analyses and the literature. The mean values are summarized in Table 1. Concerning the input variance, all four random variables of the microscale have a COV equal to 10%, while the COV of the mesoscale geometric variables (BA and UA) is selected so that the induced COV of the unit-cell volume fraction does not exceed 3%. This assumption maintains the simulation realistic, but also abides with the modeling limitation of the non-consideration of the yarns' contact and intersection.

The output variability is presented in Fig. 12. The in-plane elastic moduli E_1 and E_2 gather the highest COV levels, which makes sense due to the geometric variation of the yarns in the mesoscale. This is also related with the slight skewness introduced in the PDF shapes of those moduli, as shown in Fig. 13a and b. In this figure, the output histograms along with the PDF shapes according to the KDE method and the best fit among known probability distributions, are presented. Most of the effective properties are of Gaussian shape. The highest skewness is obtained in E_2 (Fig. 13b) and v_{12} (Fig. 13g), implying they are profoundly sensitive to the mesoscale uncertainties.

Results of the variance-based GSA are demonstrated in Fig. 14, in terms of evolution of each Sobol index (Eq. (20)) over the number of simulations. It is highlighted that this illustration is preferable in comparison with the table values after a standard number of simulations (which is the trend in the literature), in order to be certain that the indices have converged. In all subfigures there are solid lines indicating the indices limits of 0 and 1. The variance of the shear moduli (Figs. 14d, e and f) is dominated by the yarn volume fraction variability. E_2 and v_{12} are indeed governed by the braiding angle input as assumed (Figs. 14b and g) and

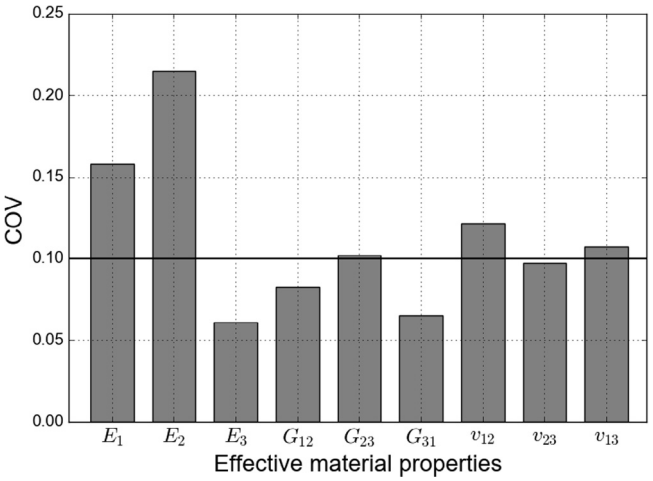

Fig. 12. Output variability for the general case.

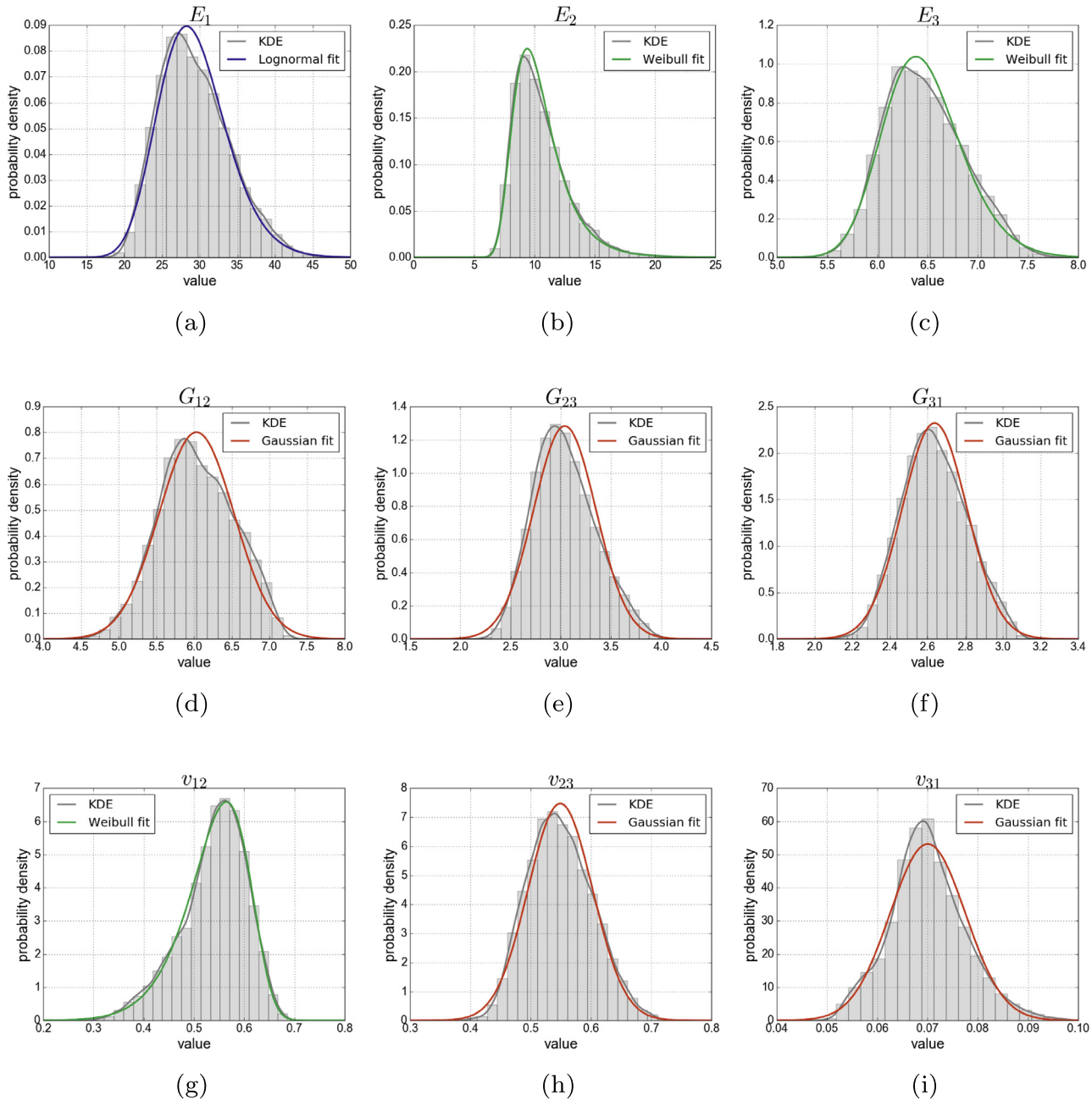

Fig. 13. Histograms of the effective mechanical properties and best fits.

the skewness of the PDFs is explained. In general, the yarn volume fraction seems as the most influential parameter, together with the braid angle. The undulation angle does not seem to have a noteworthy variability impact on the elastic properties. It is also noted that some of the output parameters required up to 8000 simulations to converge.

7. Concluding remarks

Uncertainties due to manufacturing imperfections affect the elastic behavior of braided composites. In this paper, a method is described for the effective properties prediction under uncertainty for textile composites. A multiscale model of a triaxial braided composite is presented and the effect of several micro and meso scale uncertainties is investigated. The developed algorithm is modeling a unit-cell at the mesoscale over TexGen, with homogenized yarn properties through an analytical model. Numerical homogenization is performed via ABAQUS and the effective mechanical properties are extracted with a Python post-processing script. Response variability is calculated via trained NN in the core of Monte Carlo simulation, thus results can be obtained with orders of magnitude less computational effort compared to the standard procedure. Sensitivity analysis is performed through a global technique, by measuring the contribution of the uncertain parameters to the output variance through the Sobol indices. Both material and geometric related uncertainties can be introduced. With reliable uncertainty measurements the method can solve accurately the forward uncertainty propagation problem

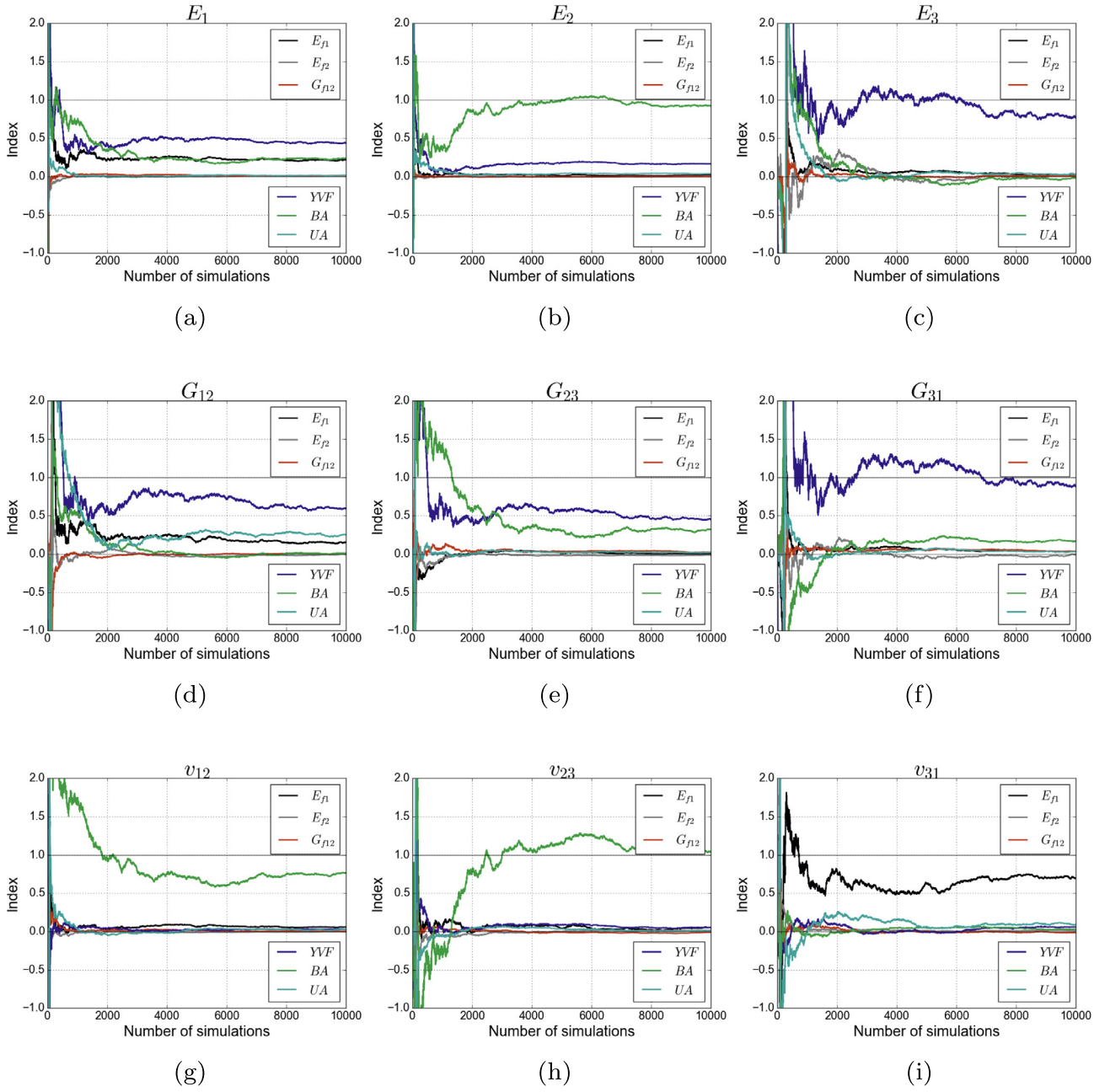

Fig. 14. Sobol indices.

and provide accurate PDFs for the effective properties of braided macrostructures, that could be later used for reliability analyses. The method can be extended to consider the contact between the yarns with an ad hoc code.

Acknowledgments

This work is implemented within the framework of the research project "FULLCOMP: Fully Integrated Analysis, Design, Manufacturing and Health-Monitoring of Composite Structures" under European Union's Horizon 2020 research and innovation program and is funded by the European Commission under a Marie Sklodowska-Curie Innovative Training Networks Grant (No. 642121) for European Training Networks (ETN). The provided financial support is gratefully acknowledged by the authors.

References

[1] Byun JH, Chou TW. Modelling and characterization of textile structural composites: A review. J Strain Anal Eng Des 1989;24(4):253–62.
[2] Lomov SV, Perie G, Ivanov DS, Verpoest I, Marsal D. Modeling three-dimensional fabrics and three-dimensional reinforced composites: challenges and solutions. Text Res J 2011;81(1):28–41.
[3] Dixit A, Mali HS. Modeling techniques for predicting the mechanical properties of woven-fabric textile composites: A review. Mech Compos Mater 2013;49(1):1–20.
[4] Ayranci C, Carey J. 2D braided composites: A review for stiffness critical applications. Compos Struct 2008;18(1):43–58.
[5] Fang G, Liang J. A review of numerical modeling of three-dimensional braided textile composites. J Compos Mater 2011;45(23):2415–36.
[6] Huang ZM. The mechanical properties of composites reinforced with woven and braided fabrics. Compos Sci Technol 2000;60(4):479–98.
[7] Tang ZX, Postle R. Mechanics of three-dimensional braided structures for composite materials – Part II: Prediction of the elastic moduli. Compos Struct 2001;51(4):451–7.

[8] Chen L, Tao XM, Choy CL. Mechanical analysis of 3-D braided composites by the finite multiphase element method. Compos Sci Technol 1999;59(16):2383–91.
[9] Zhang C, Xu X. Finite element analysis of 3D braided composites based on three unit-cells models. Compos Struct 2013;98:130–42.
[10] Zhang C, Curiel-Sosa JL, Bui TQ. A novel interface constitutive model for prediction of stiffness and strength in 3D braided composites. Compos Struct 2017;163:32–43.
[11] Zhang C, Curiel-Sosa JL, Bui TQ. Comparison of periodic mesh and free mesh on the mechanical properties prediction of 3D braided composites. Compos Struct 2017;159:667–76.
[12] Zhang C, Binienda WK, Kohlman LW. Analytical model and numerical analysis of the elastic behavior of triaxial braided composites. J Aerosp Eng 2014;27(3):473–83.
[13] Dong J, Huo N. A two-scale method for predicting the mechanical properties of 3D braided composites with internal defects. Compos Struct 2016;152:1–10.
[14] Ernst G, Vogler M, Hühne C, Rolfes R. Multiscale progressive failure analysis of textile composites. Compos Sci Technol 2010;70:61–72.
[15] Rolfes R, Vogler M, Czichon S, Ernst G. Exploiting the structural reserve of textile composite structures by progressive failure analysis using a new orthotropic failure criterion. Comput Struct 2011;89:1214–23.
[16] Sriramula S, Chryssanthopoulos K. Quantification of uncertainty modelling in stochastic analysis of FRP composites. Compos A 2009;40:1673–84.
[17] Bishara M, Rolfes R, Allix O, Revealing complex aspects of compressive failure of polymer composites – Part I: Fiber kinking at microscale. Compos Struct 2017;169:105–115.
[18] Bishara M, Vogler M, Rolfes R, Revealing complex aspects of compressive failure of polymer composites – Part II: Failure interactions in multidimensional laminates and validation. Compos Struct 2017;169:116–128.
[19] Kriegesmann B, Rolfes R, Hühne C, Temer J, Arbocz J. Probabilistic design of axially compressed composite cylinders with geometric and loading imperfections. Int J Struct Stab Dyn 2010;10(4):623–44.
[20] Kriegesmann B, Rolfes R, Hühne C, Kling A. Fast probabilistic design procedure of axially compressed composite cylinders. Compos Struct 2011;93(12):3140–9.
[21] Kamiński M, Kleiber M. Perturbation based stochastic finite element method for homogenization of two-phase elastic composites. Comput Struct 2000;78(6):811–26.
[22] Sakata S, Ashida F, Zako M. Kriging-based approximate stochastic homogenization analysis for composite materials. Comput Methods Appl Mech Eng 2008;197(21–24):1953–64.
[23] Savvas D, Stefanou G, Papadrakakis M, Deodatis G. Homogenization of random heterogeneous media with inclusions of arbitrary shape modeled by XFEM. Comput Mech 2014;54(5):1221–35.
[24] Stefanou G, Savvas D, Papadrakakis M. Stochastic finite element analysis of composite structures based on material microstructure. Compos Struct 2015;132:384–92.
[25] Kamiński M, Pawlak A. Various approaches in probabilistic homogenization of the CFRP composites. Compos Struct 2015;133:425–37.
[26] El Kadi H. Modeling the mechanical behavior of fiber-reinforced polymeric composite materials using artificial neural networks – A review. Compos Struct 2006;73:1–23.
[27] Zhang Z, Friedrich K. Artificial neural networks applied to polymer composites: a review. Compos Sci Technol 2003;63:2029–44.
[28] Dey S, Mukhopadhyay T, Adhikari S. Metamodel based high-fidelity stochastic analysis of composite laminates: A concise review with critical comparative assessment. Compos Struct 2017;171:227–50.
[29] Rouhi M, Rais-Rohani M, Najafi A. Probabilistic analysis and optimization of energy absorbing components made of nanofiber enhanced composite materials. Compos Struct 2013;100:144–53.
[30] Jansson N, Wakeman WD, Månson J-AE. Optimization of hybrid thermoplastic composite structures using surrogate models and genetic algorithms. Compos Struct 2007;80:21–31.
[31] Bui TQ, Tran AV, Shah AA. Improved knowledge-based neural network (KBNN) model for predicting spring-back angles in metal sheet bending. Int J Model Simul Sci Comput 2014;5(2):1350026.
[32] Dey S, Naskar S, Mukhopadhyay T, Gohs U, Spickenheuer A, Bittrich L, Sriramula S, Adhikari S, Heinrich G. Uncertain natural frequency analysis of composite plates including effect of noise – A polynomial neural network approach. Compos Struct 2016;143:130–42.
[33] Zhou XY, Gosling PD, Pearce CJ, Ullah Z, Kaczmarczyk L. Perturbation-based stochastic multi-scale computational homogenization method for woven textile composites. Int J Solids Struct 2016;80:368–80.
[34] Jiang D, Li Y, Fei Q, Wu S. Prediction of uncertain elastic parameters of a braided composite. Compos Struct 2015;126:123–31.
[35] Hill R. Elastic properties of reinforced solids: Some theoretical principles. J Mech Phys Solids 1963;11:357–72.
[36] Lin H, Brown LP, Long AC. Modelling and simulating textile structures using TexGen. Adv Mater Res 2011;331:44–7.
[37] Li S, Wongsto A. Unit cells for micromechanical analyses of particle-reinforced composites. Mech Mater 2004;36:543–72.
[38] ABAQUS, Documentation, Dassault Systèmes Simulia Corp. Providence RI 2014.
[39] Saltelli A, Ratto M, Andres T, Campolongo F, Cariboni J, Gatelli D, Saisana M, Tarantola S. Global sensitivity analysis. The primer. John Wiley and Sons; 2008.
[40] Sobol IM. Global sensitivity indices for nonlinear mathematical models and their Monte Carlo estimates. Math Comput Simul 2001;55:271–80.
[41] Saltelli A, Annoni P, Azzini I, Campolongo F, Ratto M, Tarantola S. Variance based sensitivity analysis of model output. Design and estimator for the total sensitivity index. Comput Phys Commun 2010;181:259–70.
[42] Sudret B. Global sensitivity analysis using polynomial chaos expansions. Reliab Eng Syst Saf 2008;93:964–79.
[43] Crestaux T, Le Maître O, Martinez JM. Polynomial chaos expansion for sensitivity analysis. Reliab Eng Syst Saf 2009;94:1161–72.
[44] Fausett L. Fundamentals of neural networks. Prentice Hall; 1994.
[45] Swingler K. Applying neural networks: a practical guide. Academic press; 1996.
[46] Chamis CC. Mechanics of composite materials: Past, present, and future. J Compos Technol Res 1989;11:3–14.
[47] MATLAB, Release 2014b, The MathWorks Inc., Natick, Massachusetts, United States; 2014.
[48] Wehrkamp-Richter T, Humbs M, Schultheiss D, Hinterhölzl R, Damage characterization of triaxial braided composites under tension using full-field strain measurement. In: The 19th international conference on composite materials. Montreal, Canada; 2013.
[49] Kelkar AD, Whitcomb JD. Technical report: Characterization and structural behavior of braided composites. U.S. Department of Transportation, Federal Aviation Administration; 2009.
[50] Klemelä J. Smoothing of multivariate data: Density estimation and visualization. Wiley; 2009.
[51] Stein M. Large sample properties of simulations using Latin hypercube sampling. Technometrics 1987;29:143–51.
[52] Sun H-Y, Qiao X. Prediction of the mechanical properties of three-dimensional braided composites. Compos Sci Technol 1996;57:623–9.
[53] Deng Y, Chen X, Wang H. A multi-scale correlating model for predicting the mechanical properties of tri-axial braided composites. J Reinf Plast Compos 2013;32(24):1934–55.